Organic & Biomolecular Chemistry

Dynamic Article Links

Cite this: *Org. Biomol. Chem.*, 2011, **9**, 2142

www.rsc.org/obc

PAPER

Fluorescent neuroactive probes based on stilbazolium dyes†

Adrienne S. Brown, Lisa-Marie Bernal, Teresa L. Micotto, Erika L. Smith‡ and James N. Wilson*

Received 7th October 2010, Accepted 13th December 2010
DOI: 10.1039/c0ob00849d

A set of spectrally diverse stilbazolium dyes was identified in an uptake assay using cultured brainstem and cerebellum cells isolated from e19 chicks. Pretreatment of cells with indatraline, a monoamine reuptake inhibitor, allowed identification of dyes that may interact with monoamine transporters. Two structurally related, yet spectrally segregated, probes, (*E*)-1-methyl-4-[2-(2-naphthalenyl)ethenyl]-pyridinium iodide (NEP+, **3A**) and (*E*)-4-[2-(6-hydroxy-2-naphthalenyl)ethenyl]-1-methyl-pyridinium iodide (HNEP+, **4A**), were selected and further investigated using HEK-293 cells selectively expressing dopamine, norepinephrine or serotonin transporters. HNEP+ was selectively accumulated *via* catecholamine transporters, with the norepinephrine transporter (NET) giving the highest response; NEP+ was not transported, though possible binding was observed. The alternate modes of interaction enable the use of NEP+ and HNEP+ to image distinct cell populations in live brain tissue explants. The preference for HNEP+ accumulation *via* NET was confirmed by imaging uptake in the absence and presence of desipramine, a norepinephrine reuptake inhibitor.

Introduction

Monoamine transporters (MATs) play critical regulatory roles removing neurotransmitters from synaptic clefts and extracellular milieu.[1,2] The serotonin transporter (SERT), dopamine transporter (DAT) and norephinephrine transporter (NET) are the targets of antidepressants and related pharmacotherapies. The side effects of many psychoactive drugs underscore the multitude of roles these neurotransmitters fulfill as well as the complexity of their expression and regulation.[3–6] The development of new classes of drugs remains a high priority with dual- and triple-acting inhibitors receive increasing interest.[7,8] Concurrent with the search for new pharmacotherapies is a drive for improving tools for screening and imaging, particularly with respect to *in vivo* or *ex vivo* assessment of transporter dynamics.[9–11] Fluorescence-based, functional assays in which probes accumulate intracellularly are of special interest as they avoid the use of radioactive materials. Furthermore, they can identify inhibitors with novel binding modes that may be overlooked in competitive binding assays.[12]

Fluorescent substrates for MATs and organic cation transporters (OCTs) have been described by several groups.[11,13–19] Hadrich[13] reported fluorescent substrates targeting neuroblastomas based on guanidine, cocaine and nisoxetine while Sames[19] recently demonstrated a coumarin-based probe as substrates of vesicular MAT. The cationic dye, 4-[4-(dimethyl amino)styryl]-*N*-methylpyridinium iodide (ASP+, Fig. 1), a fluorescent analog of the neurotoxin MPP+, serves as substrate for multiple transporter types. ASP+ was utilized as a probe of OCTs by Pietruck and coworkers,[11] while DeFelice showed that ASP+ is transported *via* DAT, NET, and to a lesser extent SERT.[16,17] The stilbazolium core of ASP+ represents a structurally broad class of fluorophores with tunable optical properties.[20–26] We anticipated that varying the identity of the electron donating vinylarene or electron accepting aryl cation components would impart different modes of cellular uptake while simultaneously introducing spectral diversity. For example, Rosania *et al.* demonstrated that members of a library of styryl-pyridinium dyes exhibited selectivity for certain subcellular compartments.[20] Probes with selectivity for a particular MAT would be useful for monitoring the activity or level of expression of a specific transporter. Ideally, a 'tool kit' of probes could be employed to target specific cell types (*i.e.* dopaminergic *vs.*

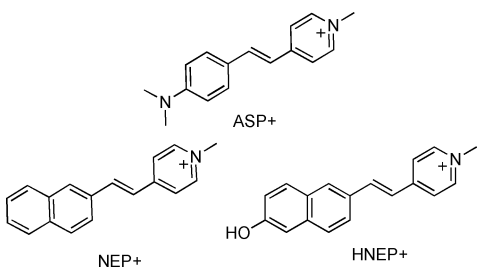

Fig. 1 The structure three stilbazolium dyes: ASP+, a known MAT and OCT substrate, NEP+ (**3A**) and HNEP+ (**4A**), described herein.

Department of Chemistry, University of Miami, 1301 Memorial Drive, Coral Gables, FL, 33124, USA. E-mail: jnwilson@miami.edu; Fax: +1 305 284 4571; Tel: +1 305 284 2619

† Electronic supplementary information (ESI) available: ^{1}H NMR, ^{13}C NMR spectra), 3D reconstructions (as .mov files). See DOI: 10.1039/c0ob00849d

‡ Present address: Princeton University, 2457 Frist Center, Princeton, NJ, 08544, USA.

serotonergic, astrocytes *vs.* neurons). Herein we describe our efforts to identify additional neuroactive probes from a family of stilbazolium dyes utilizing a cellular uptake assay, chemical inhibitors of MATs as well as directly imaging uptake of the fluorescent reporters in cell culture and live embryonic chick brain explants.

Results and discussion

Probe synthesis

N-methyl-picolinium iodide or 1,4-dimethylquinolium iodide (**A–D**) were exposed to aryl aldehydes (**1–8**) under Knoevenagel[27,28] conditions (Scheme 1) for a total of 32 reaction combinations (*i.e.* **1A–8D**); several members of this library have previously been described.[20–26] The cationic pyridinium or quinolium functionality is likely to mimic the protonated ethylamine of the native substrates. The arylaldehydes serve two roles: first, they impart chemical diversity that may lead to preferential uptake by specific transporters or cell types. Second, the aryl functionalities selected serve as electron rich substituents that may modulate the absorption and emission wavelengths. For screening purposes, the reaction isolates were utilized without further purification as the expected products were achieved with >90% purity in many cases by simply decanting the supernatant liquid; reactions involving component **B** resulted in low yields of the desired products. Compounds exhibiting high activity in cellular uptake assays, *i.e.* **2A**, **2D**, **3A**, **3D**, **4A**, **5D**, **7A** and **7D** (vide infra), were selected for purification and characterization by ^{1}H-NMR, ^{13}C-NMR, IR, HRMS, UV-vis and fluorescence spectroscopy (see Experimental).

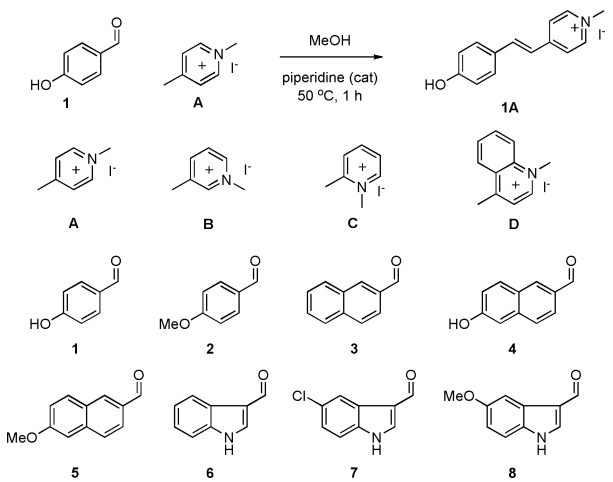

Scheme 1 Reaction conditions and building blocks used to produce the library of fluorescent arylene-vinylene probes.

Optical spectroscopy

UV-vis spectroscopy of **2A**, **2D**, **3A**, **4A**, **5D**, and **7A** in methanol reveals absorption maxima ranging from 358 nm for **2A** to 441 nm for **5D** (Fig. 2); the peaks lack vibronic structure, characteristic of intramolecular charge transfer absorption expected for donor–acceptor systems. Emission maxima range from 475 nm, in the case of **2A**, to 623 nm (**5D**) spanning much of the visible spectrum.

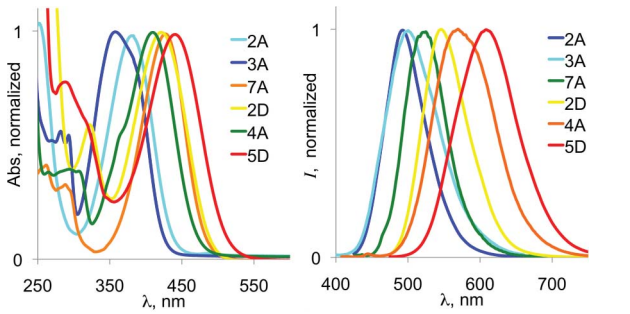

Fig. 2 Normalized absorption (left) and emission spectra (right) of selected library members (10 μM MeOH solutions). Absorption maxima vary from the near UV to blue; all dyes are compatible with 405 nm laser exciation. Emission ranges across the entire visible spectrum with large (150+ nm) Stokes shifts for several dyes.

The dyes possess large Stokes shifts of 120 to 165 nm. Compounds containing the quinolium functionality, **D**, exhibit longer absorption and emission wavelengths than the corresponding pyridinium analogs, *e.g.* **2A** *vs.* **2D** ($\lambda_{max, em}$ = 490 and 540 nm, respectively). Benzo-fusion produces a red shift in the case of **2A** *vs.* **5A**, as well. Introduction of electron donating groups also results in a bathochromic shift as in the case of **4A**, the hydroxy substituted homolog of **3A** shifting the emission maxima approximately 80 nm. Epifluorescent imaging of the probes can be accomplished using conventional filtersets such as those for DAPI and GFP. All of the dyes can be excited using a 405 nm laser, enabling confocal imaging without the need for UV specific optics. The broad range of emission wavelengths allows for selective detection of appropriately paired dyes (*i.e.* **2A** or **3A** in combination with **4A** or **5D**). Molar absorptivities (ε) ranged from 29,000 to 55,000 M^{-1}, cm^{-1} with quantum yields of photoemission (Φ_{em}) ranging from 0.20 to 0.01 (data taken in methanol). While compounds with low Φ_{em} are of limited utility, the overall brightness ($\varepsilon \cdot \Phi_{em}$) of probes utilized in imaging experiments (**3A** and **4A**, see below) compares favorably with other fluorescent probes such as acridine orange, Hoescht 33258 and DAPI.

Cellular uptake and inhibition studies

The native fluorescence of the probes enables direct detection of their uptake in dissociated e19 chick brain cells in a convenient 96-microwell plate format; this method allows us to screen for activity against multiple cell types and transporters including MATs and OCTs without the use of radioactive compounds.[15,18,29,30] Solutions of **1A–8D** were prepared from the reaction isolates to produce a probe concentration of approximately 100 μM; incubation time was 10 min. The fluorophore solution was removed, fresh media added and the plate immediately analyzed by a microwell plate reader. Given the broad range of absorption and emission wavelengths, excitation varied from 355 nm to 500 nm with emission collected at +100 nm to +150 nm. Twelve of the thirty-two compounds screened were found to associate with the cultured cells in this initial assay (Fig. 3) based on an increase in emission intensity of 3× compared to untreated cells. Components **A** and **D** are well represented, while only two examples of **B** and no compounds possessing **C**, **6** or **8** were detected in this screen. This may be due to a combination of factors including low uptake, low

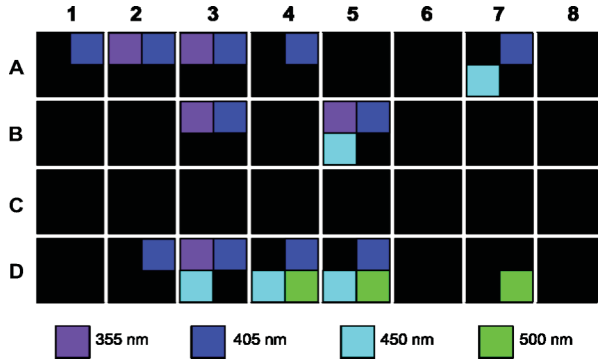

Fig. 3 Fluorescent probes identified in uptake assay utilizing dissociated whole brain cells harvested from e19 chicks; excitation wavelength key at bottom, emission was collected at +100 to +150 nm. Conditions detailed in Experimental.

brightness, poor reaction yields or high cytotoxicity resulting in cell detachment and removal during the washing step. Overall, a small fraction of the reactions proved to produce compounds with high brightness ($\varepsilon \times \Phi$) and high bioactivity. However, it is likely that many more neuroactive stilbazolium with attractive optical properties could be identified in larger libraries or through rational design.

From this initial assay we are only able to determine if a compound associates with the cultured cells; it is not clear if a particular probe is actively transported into cells or simply interacts with the cell membrane. The use of the MAT reuptake inhibitor, indatraline, provides some insight into what mechanisms of cellular uptake are at play. Dissociated brain cells were pretreated with indatraline then the dye solutions as described above. The emission response of several probes was affected by indatraline pretreatment, including **2D**, **3A**, and **4A** suggesting that at least one mode of cellular uptake for these compounds is *via* a MAT. In contrast, probes **2A**, **3D**, **5D**, **7A** and **7D** maintained high responses in spite of indatraline pretreatment (Fig. 4), indicating these probes either simply interact with the cell membrane, or are accumulated *via* other transporters, *i.e.* OCTs. The remaining combinations possessed weak responses or low overall intensity and were not characterized further.

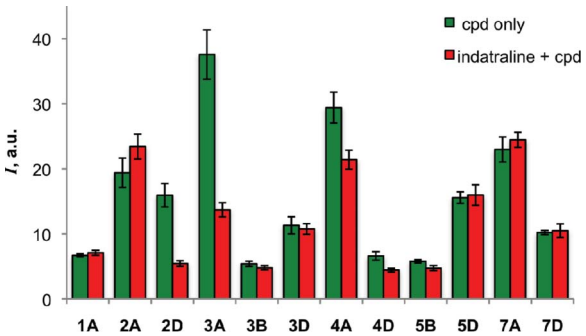

Fig. 4 Relative uptake based on emission intensities of stilbazolium dyes in e19 chick whole brain cultures in the absence and presence of indatraline, a monoamine reuptake inhibitor (mean of six experiments; error bars show SEM).

Live cell and tissue imaging

The two brightest compounds inhibited by indatraline, **3A** and **4A**, were selected for examination in live brain explants as well as cell lines expressing specific MATs in order to evalute their use as probes of MAT function. HEK-293 cells stably expressing hDAT, hNET and hSERT were provided by Prof. R. Blakely[5,16,31] and cultured on 35 mm dishes with a coverslip imaging window for confocal microscopy (see Experimental). Baseline images for each cell type were taken to establish the level of cell autofluorescence, then stock solutions of probe were introduced to produce final concentrations ranging from 10 μM to 100 μM; laser intensity and gain were not altered for subsequent images captured at 10 s intervals. Representative images are shown in Fig. 5 together with intensity profiles captured from cell bodies. Time course images reveal that **4A** is rapidly accumulated by HEK-hNET and to a lesser extent by HEK-hDAT. Based on the time dependent intensity profiles, the response towards HEK-hSERT cells does not differ substantially from control untransfected HEK cells. Inspection of images obtained for DAT and SERT cells reveals

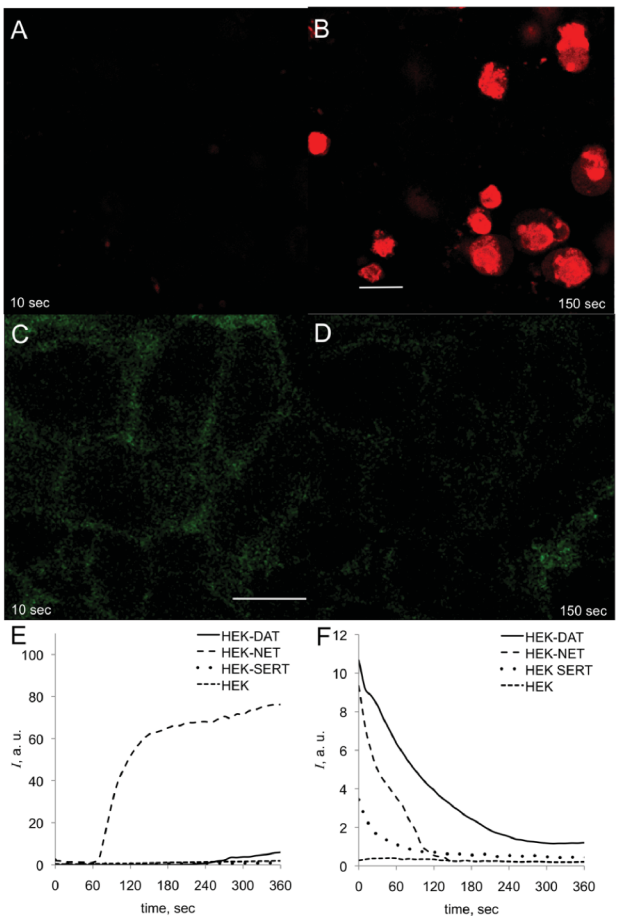

Fig. 5 The contrasting behaviour of **3A** and **4A** towards HEK293 cells expressing DAT, NET or SERT. **4A** preferentially accumulates in cells expressing NET as revealed by time-lapse fluorescence microscopy; panel A, 10 s (immediately after introduction of **4A**), panel B 150 s (scale bar is 10 μm). By contrast, **3A** did not accumulate in cells expressing DAT, NET or SERT, though binding may occur at DAT or SERT (panel C, 10 s) with emission intensity decreasing with time due to photobleaching (D, 150 s). Time-dependent intensity plots are shown in E, F.

that **4A** may be binding to these transporters as fluorescent halos[32] were observed, however, transport does not appear to occur in the case of SERT and at a much slower rate (and delayed onset) in the case of DAT. By contrast, **3A** does not appear to be transported *via* DAT, NET or SERT. **3A** may bind to cells expressing these transporters, however, we did not observe an increase of emission intensity within the cell bodies and instead a slow loss of fluorescence due to photobleaching was observed (Fig. 5). The time dependent imaging of **4A** reveals a preference for NET, similar to ASP+.[16,17] However in contrast to ASP+, **4A** does not appear to be transported *via* SERT making this a selective catecholaminergic probe with a high level of discrimination between DAT and NET.

We next examined **3A** and **4A** in live brainstem and cerebellum sections to determine their distribution in a complex, multicellular environment. Fig. 6 (A,B) shows cerebellum sections treated individually with **3A** and **4A**; **3A** appears to be more widely distributed than **4A**, though both dyes are limited to discreet cell populations tracing the cerebellar gyri. This distribution is consistent with the behavior of these probes towards MAT-expressing HEK293 cells. The wider distribution of **3A** may be due to binding to multiple transporter types including MATs, OCTs or cationic aminoacid transporters[34] (CATs), while **4A** may be limited to NET or DAT expressing catecholaminergic cells. The spectral segregation of **3A** and **4A** enables their simultaneous use to identify cells that differentially accumulate each probe. Image overlays from 100 μm sagittal (Fig. 6A) and transverse (Fig. 6B) sections[33] reveal that both probes are associated with cells of chick mesencephalon and metencephalon. The fluorophores were excited at 405 nm; the emission of **3A** (in green) was collected between 425 and 500 nm, the emission of **4A** (in red) was collected from 575 to 650 nm with areas of overlap appearing as yellow. **3A** is widely distributed in both the cerebellum and pons while **4A** appears in distinct cell groupings along the cerebellar gyri and around the midline of the brainstem especially in multiple tract-like sructures. The chick brainstem possesses dense clusters of chatecholaminergic[35,36] and serotonergic[37] cells that project into the cerebellum and front brain. We observed both perikarya and fibers stained with **4A** in this region with several discreet cell clusters brightly illuminated (Fig. 6C). Pretreatment of brain sections with desipramine, a norepinephrine reuptake inhibitor, limited the accummulation of **4A** (Fig. 7), consistent with the results observed for hNET-expressing HEK-293 cells. Visual inspection of the images reveals a distinct difference between desipramine treated (Fig. 7B) and untreated (Fig. 7A) tissue that

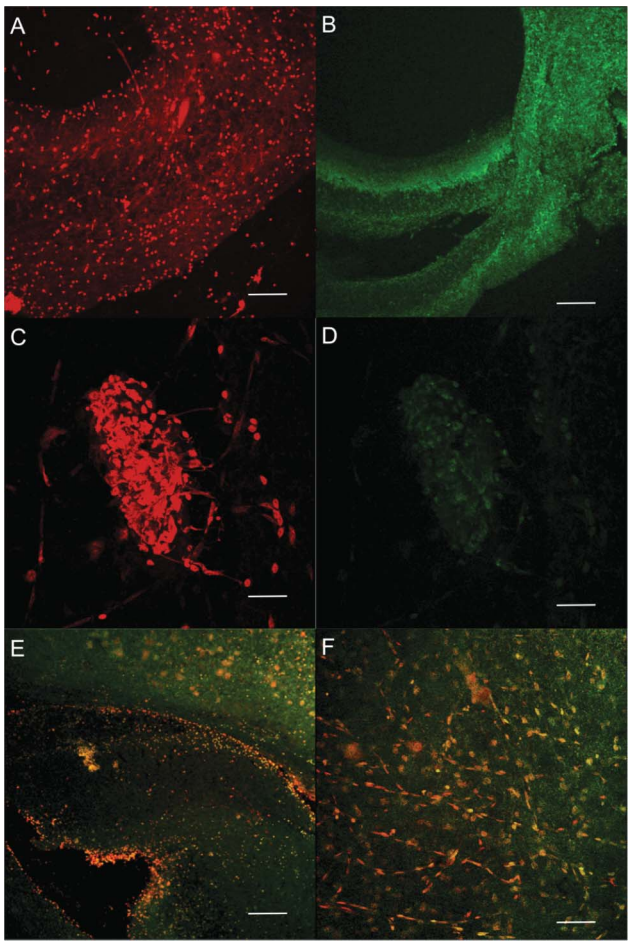

Fig. 6 Confocal microscopy images of live e19 chick brain explants treated with **3A** (green) and **4A** (red). 3D overlays of sequential transverse cerebellum sections (panels A,B scale bar: 100 μm) demonstrate that **4A** is largely accumulated in discreet cell bodies while the distribution of **3A** is more diffuse. Transverse sections of the metencephalonic brain stem reveal discrete clusters of cells that accumulate **4A** (C, scale bar: 10 μm) visible both in the cell bodies and processes; **3A** association with the same cells is minimal (D). The spectral segregation of **3A** and **4A** enables their simultaneous to image cells that differentially accumulate each probe in the metencephalon (E, F, scale bar: 50 μm); while **3A** is broadly distributed, **4A** is localized to distinct clusters and tracts.

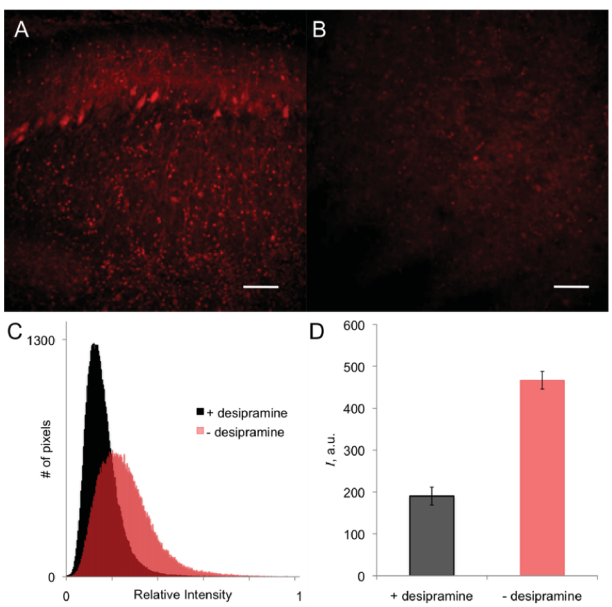

Fig. 7 *Ex vivo* assessment of **4A** uptake in the absence and presence of the norepinephrine reuptake inhibitor, desipramine. Sequential sections of e19 chick cerebellum were treated with **4A** alone (40 μM, 10 min; panel A, scale bar is 100 μm) or pretreated with desipramine (10 μM, 3 min) then **4A** (B). In the absence of desipramine, **4A** accumulates in cell bodies and processes while desipramine pretreatment severely attenuates uptake leaving only diffuse distribution. Histogram of pixel intensity (C) for desipramine dependent **4A** uptake; mean intensity (D), 5 sections, error bars show SEM. Laser intensity and detector gain were kept constant while obtaining images.

correlates with image analysis: While individual cell bodies and processes are visible in cells exposed to **4A**, pretreatment with desipramine limits the overall emission intensity (Fig. 7D) and the lack of accumulation to discreet structures or cells is evident in intensity histograms (Fig. 7C).

Conclusions

We have identified a fluorescent stilbazolium dye, HNEP+, that is a highly selective NET substrate suitable as an imaging agent and reporter of transporter function both *in vitro* and ex vivo. Given the complex modes of transporter regulation,[38] the ability to monitor transporter function in tissue explants (or *in vivo*) may lead to improved assays and identification of new classes or improved selectivity of reuptake inhibitors. Our results support the notion that the MATs are capable of transporting molecular reporters that mimic certain aspects of the parent substrates. The necessity for dyes possessing high brightness ($\varepsilon \cdot \Phi_{em}$) is apparent, as only HNEP+ and NEP+ proved useful for *in vitro* and *ex vivo* imaging. We have demonstrated that subtle changes in structure lead to pronouced differences in behavior towards MATs: no accumulation of NEP+ was observed for DAT, NET or SERT expressing HEK293 cells. We anticipate that identified probes herein, as well as additional neuroactive fluorophores based on the styryl-pyridinium core, will compliment ASP+ in fluorescence based assays and imaging applications.

Experimental

Materials and methods

Reagents were obtained from Sigma Aldrich and TCI America and used without further purification. ACS reagent grade solvents were obtained from EMD Chemicals. ^{1}H and ^{13}C NMR spectra were obtained on a Bruker 500 MHz spectrometer using tetramethylsilane TMS as the internal standard and DMSO as the solvent. Absorbance spectra were recorded on a Perkin–Elmer Lambda 35 UV-vis spectrometer; emission spectra were recorded on a Perkin–Elmer LS55 Fluorometer. For determination of Φ_{em}, solutions were prepared to an optical density of 0.05 or less in MeOH to minimize inner filter effects. Perylene in cyclohexane was used as a reference for quantum yields.[39]

All procedures and experiments involving embryonic chick derived cells and tissue are in compliance with University of Miami Institutional Animal Care & Use Committee.

Synthesis

The syntheses of compounds **1A–D**,[21,24,26] **2A–D**,[21,24,26] **3A**[22] and **6A**[23] have been previously described. In a typical reaction, 0.5 mmol of N-methylpicolinium iodides (**A–C**) or 1, 4-dimethylquinolinium iodide was placed in a 20 mL scintillation vial equipped with a microstribar, followed by 0.55 mmol (1.1 eq) of the appropriate aldehyde, methanol (10 mL) and 3 drops of piperidine. The reaction vessel was capped, stirred and heated at 65 °C for 2–3 h. The reaction mixture was allowed to reach room temperature at which point most compounds precipitated; compounds not observed to precipitate were kept at 4 °C overnight. Acetic acid was added to those reactions involving aldehydes with hydroxyl groups. In some cases, the addition of ethyl acetate was necessary to induce precipitation. The supernatant liquid was decanted, the product rinsed, then collected over filter paper, dried under vacuum and stored in a dessicator. For screening purposes, the crude reaction isolate was used directly. Compounds **2A**, **2D**, **3A**, **3D**, **4A**, **5D**, **7A** and **7D**, identified from reaction mixtures that demonstrated high activity (vide supra) were further purified by crystallization from MeOH; their characterization data is presented below.

(*E*)-4-[2-(4-Hydroxyphenyl)ethenyl]-1-methylpyridinium iodide (2A). IR ν_{max}: 831, 985, 1020, 1112, 1168, 1261, 1470, 1514, 1571, 1589, 3048, 3402 cm^{-1}. ^{1}H NMR (500 MHz, DMSO): δ 3.81 (3H, s), 4.22 (3H, s), 7.03 (2H, d, J = 8.5 Hz), 7.36 (1H, d, J = 16.5 Hz), 7.71 (2H, d, J = 8.5 Hz), 7.98 (1H, d, J = 16.5 Hz), 8.16 (2H, d, J = 6.5 Hz), 8.81 (2H, d, J = 6.0). ^{13}C NMR (125.74 MHz, DMSO): δ 47.24, 55.93, 115.12, 121.16, 123.48, 128.25, 130.46, 141.02, 145.32, 153.31, 161.64. Φ_{em} = 0.011, ε = 46,000 M^{-1}, cm^{-1}. HRMS (ES+) calcd for $C_{15}H_{16}NO^{+}$: 226.1232 Found: 226.1228 (E = 1.8 ppm). MP: 210 °C (dec.) Yield: 62 mg (34%)

(*E*)-4-[2-(4-Methoxyphenyl)ethenyl]-1-methylquinolium iodide (2D). IR ν_{max}: 753, 776, 824, 834, 978, 1020, 1168, 1224, 1257, 1566, 3024 cm^{-1}. ^{1}H NMR (500 MHz, DMSO): δ 3.85 (3 H, s), 4.52 (3 H, s), 7.09 (2H, d, J = 8.5 Hz), 7.98 (2 H, d, J = 9.0 Hz), 8.02 (1 H, t, J = 7.5 Hz), 8.18–8.27 (3 H, m), 8.42 (1 H, d, J = 8.5), 8.45 (1 H, d, J = 6.5 Hz), 9.06 (1 H, d, J = 8.5 Hz), 9.30 (1 H, d, J = 6.5). ^{13}C NMR (125.74 MHz, DMSO): δ 45.01, 55.97, 115.07, 116.01, 117.62, 119.79, 126.64, 126.95, 128.71, 129.56, 131.36, 135.38, 139.23, 143.47, 148.27, 153.35, 162.01. Φ_{em} = 0.012, ε = 33,000 M^{-1}, cm^{-1}. HRMS (ES+) calcd for $C_{19}H_{18}NO^{+}$: 276.1388 Found: 276.1385 (E = 1.1 ppm). MP: 271 °C (dec.) Yield: 87 mg (43%)

(*E*)-1-Methyl-4-[2-(2-naphthalenyl)ethenyl]pyridinium iodide (3A). IR ν_{max}: 746, 813, 823, 863, 873, 966, 1180, 1192, 1517, 1614, 3023 cm^{-1}. ^{1}H NMR (500 MHz, DMSO): δ 4.27 (3H, s), 7.58–7.61 (2H, m), 7.67 (1H, d, J = 16.0 Hz), 7.95–8.03 (4H, m), 8.16 (1H, d, J = 16.5 Hz), 8.21 (1H, s), 8.27 (2H, d, J = 5.5 Hz), 8.88 (2H, d, J = 6.0 Hz). ^{13}C NMR (125.74 MHz, DMSO): δ 47.43, 124.01, 124.11, 124.16, 127.46, 127.96, 128.25, 129, 129.24, 130.01, 133.29, 133.39, 134.19, 141.01, 145.61, 152.86. Φ_{em} = 0.18, ε = 32,000 M^{-1}, cm^{-1}. HRMS (ES+) calcd for $C_{18}H_{16}N^{+}$: 246.1283 Found: 246.1278 (E = 2.0 ppm). MP: 279–281 °C (dec.). Yield: 121 mg (65%)

(*E*)-1-Methyl-4-[2-(2-naphthalenyl)ethenyl]quinolinium iodide (3D). IR ν_{max}: 752.09, 826.83, 958.06, 1111.73, 1300.92, 1532.52, 1566.79, 1593.56, 3014.8, 3416.7 cm^{-1}. ^{1}H NMR (500 MHz, DMSO): δ 4.56 (3H, s), 7.61 (2H, t, J = 3.5 Hz), 7.98–8.1 (4H, m) 8.29 (3H, m) 8.32 (1H, d, J = 16.0 Hz), 8.45 (2H, m), 8.56 (1H, d, J = 6.1 Hz), 9.11 (1H, d, J = 8.1 Hz), 9.40 (1H, d, J = 6.0 Hz). ^{13}C NMR (125.74 MHz, DMSO): δ 45.22, 116.73, 119.73, 120.52, 124.91, 126.70, 126.98, 127.33, 128.01, 128.17, 128.97, 128.99, 129.70, 130.84, 133.25, 134.12, 135.41, 135.58, 139.10, 143.15, 148.43, 152.71. Φ_{em} = 0.08, ε = 29,000 M^{-1}, cm^{-1}. HRMS (ES+) calcd for $C_{22}H_{18}N^{+}$: 296.1434 Found: 296.1436 (E = 0.7 ppm). MP: 239 (dec.) Yield: 106 mg, 51%.

(*E*)-4-[2-(6-Hydroxy-2-naphthalenyl)ethenyl]-1-methyl-pyridinium iodide (4A). IR ν_{max}: 660, 805, 824, 868, 961, 1154, 1174, 1271, 1480, 1604, 3036, 3159 cm^{-1}. ^{1}H NMR (500 MHz, DMSO):

δ 4.24 (3H, s), 7.14 (1H, d, J = 8.5 Hz), 7.17 (1H, s), 7.54 (1H, d, J = 16.5 Hz), 7.78 (1H, d, J = 8.5 Hz), 7.83–7.85 (2H, m), 8.07 (1H, s), 8.11 (1H, d, J = 16.0 Hz), 8.21 (2H, d, J = 7.0 Hz), 8.83 (2H, d, J = 7.0 Hz), 10.13 (1H, s). ^{13}C NMR (125.74 MHz, DMSO): δ 47.28, 109.58, 119.92, 122.33, 123.64, 124.34, 127.50, 127.87, 130.18, 130.55, 130.91, 136.17, 141.61, 145.41, 153.14, 157.50. Φ_{em} = 0.106, ε = 38,000 M^{-1}, cm^{-1}. HRMS (ES+) calcd for $C_{14}H_{14}NO^+$: 262.1232 Found: 262.1235 (E = 1.1 ppm) MP: 286–290 °C, 270 °C color change (yellow→orange). Yield: 88 mg (45%)

(*E*)-4-[2-(6-Methoxy-2-naphthalenyl)ethenyl]-1-methylquinolinium iodide (5D). IR ν_{max}: 749, 758, 813, 823, 855, 969, 1168, 1191, 1518, 1614, 3020 cm^{-1}. ^{1}H NMR (500 MHz, DMSO): δ 3.92 (3H, s), 4.54 (3H, s), 7.23 (1H, dd), 7.41 (1H, d, J = 2.0 Hz), 7.91 (1H, t), 7.94 (1H, t), 8.06 (1H, t, J = 2.0 Hz), 8.22 (1H, d, J = 9.0 Hz), 8.21–8.32 (3H, m), 8.38 (1H, d, J = 15.5 Hz), 8.44 (1H, d, J = 9), 8.52 (1H, d, J = 6.5 Hz), 9.09 (1H, d, J = 8.5 Hz), 9.34 (1H, d, J = 6.5 Hz). ^{13}C NMR (125.74 MHz, DMSO): δ 45.12, 55.88, 106.85, 116.42, 119.34, 119.83, 119.87, 125.52, 126.75, 126.96, 128, 128.7, 129.67, 130.77, 130.94, 131.45, 135.43, 136.08, 139.22, 143.70, 148.44, 153.05, 159.19. Φ_{em} = 0.11, ε = 30,000 M^{-1}, cm^{-1}. HRMS (ES+) calcd for $C_{23}H_{20}NO^+$: 326.1545 Found: 326.1544 (E = 0.3 ppm). MP: 269–272 °C (dec.) Yield: 61 mg (27%).

(*E*)-4-[2-(5-Chloro-1*H*-indol-3-yl)ethenyl]-1-methylpyridinium iodide (7A). IR ν_{max}: 672, 748, 810, 821, 860, 967, 1185, 1421, 1593, 1607, 3027, 3174 cm^{-1}. ^{1}H NMR (500 MHz, DMSO): δ 4.17 (3H, s), 7.23 (1H, d, J = 8.5 Hz), 7.27 (1H, d, J = 16.5 Hz), 7.50 (1H, d, J = 8.5 Hz), 8.05 (1H, s), 8.13 (2H, d, J = 6.5 Hz), 8.20 (1H, s), 8.23 (1H, d, J = 17.0 Hz), 8.70 (2H, d, J = 6.5 Hz), 12.05 (1H, s). ^{13}C NMR (125.74 MHz, DMSO): δ 46.81, 113.60, 114.51, 117.94, 119.93, 122.28, 123.26, 126.30, 126.65, 133.16, 135.64, 136.24, 144.70, 154.43. Φ_{em} = 0.018, ε = 40,000 M^{-1}, cm^{-1}. HRMS (ES+) calcd for $C_{16}H_{14}ClN_2^+$: 269.0846 Found: 269.0851 (E = 1.9 ppm). MP: 279–281 °C (dec.), 230 °C color change (yellow→orange), Yield: 60 mg (30%).

(*E*)-4-[2-(5-Chloro-1*H*-indol-3-yl)ethenyl]-1-methylquinolium iodide (7D). IR ν_{max}: 671.00, 751.88, 893.10, 1024.17, 1050.02, 1112.44, 1134.70, 1221.66, 1309.30, 1394.64, 1515.93, 1589.25, 3161.8 cm^{-1}. ^{1}H NMR (500 MHz, DMSO): δ 4.43 (3H, s), 7.23 (1H, d, J = 7.0 Hz), 7.49 (1H, d, J = 8.0 Hz), 7.98 (2H, m), 8.19 (2H, m), 8.29 (1H, d, J = 8.5 Hz), 8.48 (3H, m), 8.94 (2H, d, J = 8.0 Hz), 9.12 (1H, d, J = 5.5 Hz). ^{13}C NMR (125.74 MHz, DMSO): δ 44.70, 114.14, 114.28, 114.47, 114.51, 119.43, 119.53, 123.23, 125.92, 126.44, 126.71, 127.66, 128.97, 132.77, 135.03, 135.86, 137.61, 139.20, 147.2, 154.00. Φ_{em} = 0.008, ε = 41,000 M^{-1}, cm^{-1}. HRMS (ES+) calcd for $C_{20}H_{16}ClN_2^+$: 319.1002 Found: 319.1007 (E = 1.5 ppm). MP: 285 °C (dec.) Yield: 69 mg (31%).

Microwell plate preparation and microwell plate assays

Brains were isolated from e19 chick embryos and plated on 96-well plates following a previously reported procedure.[18] Plates incubate for 72 h before screening. For the initial screening, fluorescent probes were added in 200 µL neuronal media (NM, Sciencell 1521 containing basal medium, neuronal growth supplement, and penicillin/streptomycin supplement) to obtain final concentrations of 100 µM and incubated for 10 min. Plates were then rinsed and 200 µL NM was added and left in each well. The microwell plates were read on a Perkin–Elmer LS55 Fluorometer equipped with a plate reader attachment; the excitation and emissions set based on the optical properties of each compound. A second round of screening exposed cells to the reuptake inhibitor, indatraline, with an incubation period of 10 min prior to exposure to the compounds. The inhibitor was added to 200 µL of media to reach a concentration of 100 µM, followed by probe addition and rinsing steps described above.

Midbrain and hindbrain isolation

The mesencephelon, metencephalon and myelencephalon were isolated from e19 chick embryos and placed in an aluminium foil mold. The tissue was submerged in 2.5% low melting point agarose gel (Invitrogen LMP Agarose, Ultrapure #5517–014) and placed on ice to solidify. A Polaron H1200 Vibrating Microtome was used to section the brain into approximately 100 µm slices. Once the gel was solidified, the block was removed from the foil mold and excess agarose gel was removed with a razor blade. The block was then positioned on the stage of the microtome using instant dry glue and allowed to dry before it was submerged in Dulbecco's Phosphate Buffered Saline solution (DPBS, Mediatech #21-031-CV) at 0 °C. To obtain sagittal section the anterior side of the cube was positioned facing up. Transverse slices were taken in 100 µm increments starting at the anterior edge of the mesencephalon and continuing posteriorly to the hindbrain. Brain regions were determined using the stereotaxic atlas of the chick brain[32] however, exact coordinate positions varied due to differences in developmental stages. Slices from the mesencephelon and metencephalon were retrieved using an inoculating loop and placed onto an 8 chamber glass vessel tissue culture treated glass slide (Cultureslide, BD Falcon, 354118) with 500 µL of NM. Sagittal slices were obtained in the same manner. Slices from the sagittal midline were retrieved and placed onto the cover slip slides. The brain sections were then treated with the fluorescent probes. Probes were added to the media to reach a concentration of 100 µM and allowed to incubate for 10 min. The tissue slices were then rinsed using an 18 gauge aspirating needle to remove the media. 50 µL of media was then added back to the tissue. The chamber compartments were then removed and the tissue was covered with a 24 × 60 mm micro cover glass (micro cover glass, VWR#48393252) and sealed using clear nail polish.

Confocal imaging

Imaging was performed on a Leica SP5 confocal microscope housed within the UM Biology Imaging Core Facility. A 405 nm diode laser was used as the excitation source. XYZ-Scans were collected with 2 µm sections. Images were analyzed using ImageJ 1.41 software (NIH, USA). 3D reconstructions of the sections displayed in Fig. 6 are available as separate files.†

Acknowledgements

We thank Prof. K. Tosney, L. White and A. Hayward (UM, Biology) for helpful discussions and assistance with live tissue preparations.

Notes and references

1 G. E. Torres, R. R. Gainetdinov and M. G. Caron, *Nat. Rev. Neurosci.*, 2003, **4**, 13.
2 J. Masson, C. Sagne, M. Hamon and El Mestikawy, *S. Pharmacol. Rev.*, 1999, **51**, 439.
3 J. R. LaCasse and J. Leo, *PLoS Med.*, 2005, **2**, e392.
4 E. Trindade, D. Menon, L.-A. Topfer and C. Coloma, *CMAJ*, 1998, **159**, 1245.
5 S. Ramamoorthy, E. Giovanetti, Y. Qian and R. D. Blakely, *J. Biol. Chem.*, 1998, **273**, 2458.
6 F. Magnani, C. G. Tate, S. Wynne, C. Williams and J. Haase, *J. Biol. Chem.*, 2004, **279**, 38770.
7 M. J. Millan, *Neurotherapeutics*, 2009, **6**, 53.
8 R. C. Shelton, *J. Clin. Psychiatry*, 2004, **65**(Supplement 17), 5.
9 R. Wagstaff, M. Hedrick, J. Fan, P. D. Crowe and D. DiSepio, *J. Biomol. Screening*, 2007, **12**, 436.
10 S. Jørgensen, E. Ø. Nielsen, N. Dan, D. Peters and T. J. Dyhring, *Neurosci. Methods*, 2008, **169**, 168.
11 M. Hörbelt, C. Wotzlaw, T. A. Sutton, B. A. Molitoris, T. Philipp, A. Kribben, J. Fandrey and F. Pietruck, *Kidney Int.*, 2007, **72**, 422.
12 M. D. Petersen, S. V. Boye, E. H. Nielsen, J. Willumsen, S. Sinning, O. Wiborg and M. Bols, *Bioorg. Med. Chem.*, 2007, **15**, 4159.
13 D. Hadrich, F. Berthold, E. Steckhan and H. Bonisch, *J. Med. Chem.*, 1999, **42**, 3101.
14 T. Mehrens, S. Lelleck, I. Cetinkaya, M. Knollmann, H. Hohage, V. Gorboulev, P. Boknik, H. Koepsell and E. Schlatter, *J. Am. Soc. Nephrol.*, 2000, **11**, 1216.
15 A. Fowler, N. Seifert, V. Acker, T. Woehrle, C. Kilpert and D. J. de Saizieu, *J. Biomol. Screening*, 2006, **11**, 1027.
16 J. W. Schwartz, R. D. Blakely and L. J. DeFelice, *J. Biol. Chem.*, 2002, **278**, 9768.
17 J. W. Schwartz, G. Novarino, D. W. Piston and L. J. DeFelice, *J. Biol. Chem.*, 2005, **280**, 19177.
18 T. L. Micotto, A. S. Brown and J. N. Wilson, *Chem. Commun.*, 2009, 7548.
19 N. G. Gubenator, H. Zhang, R. G. W. Staal, E. V. Mosharov, D. B. Pereira, M. Yue, V. Balsanek, P. A. Vadola, B. Mukherjee, R. H. Edwards, D. Sulzer and D. Sames, *Science*, 2009, **324**, 1441.
20 G. R. Rosania, J. W. Lee, L. Ding, H.-S. Yoon and Y.-T. Chang, *J. Am. Chem. Soc.*, 2003, **125**, 1130.
21 A. P. Phillips, *J. Org. Chem.*, 1949, **14**, 302.
22 C. J. Cavallito, H. S. Yun, J. C. Smith and F. F. Foldes, *J. Med. Chem.*, 1969, **12**, 134.
23 N. C. Nishimura, X.-M. Duan, K. Komatsu, S. Okada, H. Oikawa, H. Matsuda and H. Nakanishi, *MCLC S&T, Sec. B, Nonlinear Optics*, 1999, **22**, 247.
24 H. Erdtman and A. Rosengren, *Acta Chem. Scand.*, 1968, **22**, 1475.
25 A. M. Akkerman and H. Veldstra, *Recl. Trav. Chim. Pays-Bas*, 2010, **73**, 629.
26 M. S. A. Abdel-Mottaleb, M. H. Abdel-Kader and S. T. El-Araby, *Photochem. Photobiol., Proc. Int. Conf.*, 1983, **2**, 1329.
27 E. Knoevenagel, *Ber. Dtsch. Chem. Ges.*, 1898, **31**, 2550.
28 K. Sato, K. Kano, T. Yafune, M. Hida, S. Arai and T. Yamagishi, *Heterocycles*, 1994, **37**, 955.
29 S. C. Bondy and J. L. Purdy, *Brain Res.*, 1977, **119**, 403.
30 K. A. Kalesh, K. Liu and S. Q. Yao, *Org. Biomol. Chem.*, 2009, **7**, 5129.
31 A. Galli, L. J. DeFelice, B. J. Duke, K. R. Moore and R. D. Blakely, *J. Exp. Biol.*, 1995, **198**, 2197.
32 M. P. Mahaut-Smith, D. Thomas, A. B. Higham, J. A. Usher-Smith, J. F. Hussain, J. Martinez-Pinna, J. N. Skepper and M. J. Mason, *Biophys. J.*, 2003, **84**, 2646.
33 W. J. Kuenzel and M. Masson, *A Stereotaxic Atlas of the Brain of the Chick (Gallus domesticus)*, Johns Hopkins University Press, Baltimore, 1988.
34 E. I. Closs, J.-P. Boissel, A. Habermeier and A. Rotmann, *J. Membr. Biol.*, 2007, **213**, 67.
35 L. Moons, J. van Gils, E. Ghijsels and F. Vandesande, *J. Comp. Neurol.*, 1994, **346**, 97.
36 K. M. Knigge and D. T. Piekut, *Peptides*, 1985, **6**, 97.
37 N. Okado, H. Sako, S. Homma and K. Ishikawa, *Prog. Neurobiol.*, 1992, **38**, 93.
38 R. D. Blakely, L. J. DeFelice and A. Galli, *Physiology*, 2005, **20**, 225.
39 I. B. Berlman, *Handbook of Fluorescence Spectra of Aromatic Molecules*, 2nd Ed., Academic Press, New York, 1971.

